DOI: 10.67867/ccj.2026v10i3.03

September 2026; 10(3): 10-24

ChemClass Journal

Publication of the Chemical Society of Nigeria, Zaria Chapter

Journal homepage: https://chemclassjournal.com.ng

e-ISSN: 3092-8214; p-ISSN: 3092-8206

Research Article

Copper-based metal-organic framework (Cu-BDC MOF) for removal of pharmaceutical pollutants from aqueous solutions

Shangkum Yildun Goji[1]*, Nathaniel Jirgi Shamle[1], John Ikechukwu[1], Gurumji Rotbe[2], Roland Tuamyen Hoomkwap[1], Rabiat Abdullahi Lawal[1], Ohwimu Joseph Godday[3]

[1] Department of Chemistry, Faculty of Natural Sciences, University of Jos, P.M.B 2084, Jos, Plateau State, Nigeria
[2] Plateau State College of Agriculture, Garkawa, P.M.B 001, Mikang, Plateau State, Nigeria
[3] Department of Chemistry, Federal University of Petroleum Resources, Effurun, Delta State, Nigeria

OPEN ACCESS

***Corresponding Author**
Goji S.Y.
gojis@unijos.edu.ng
Phone: +234-806-456-2780
ORCID:

Article History
Received: June 02, 2026
Reviewed: June 21, 2026
Revised: July 05, 2026
Accepted: July 09, 2026
Published: September 30, 2026

Citation
Goji S.Y., Shamle N.J., Ikechukwu J., Rotbe G., Hoomkwap R.T., Lawal R.A., Ohwimu & Godday J. (2026). Copper-based metal-organic framework (Cu-BDC MOF) for removal of pharmaceutical pollutants from aqueous solutions. *ChemClass Journal,* 10(3), 10–24. DOI: 10.67867/ccj.2026v10i3.03

Copyright © 2026 Goji S.Y. et al. Published by CSN Zaria Chapter. This is an open-access article distributed under the Creative Commons Attribution License (CC BY 4.0), which permits unrestricted use, distribution, and reproduction in any medium, provided the original work is properly cited.

ABSTRACT

The discharge of pharmaceutical emerging contaminants into aquatic environments poses serious ecological and public health risks, including antimicrobial resistance. In this study, a copper-based metal-organic framework (Cu-BDC MOF) was synthesized solvothermally using terephthalic acid (benzene-1,4-dicarboxylate, BDC) as the organic linker and evaluated as an adsorbent for the simultaneous removal of promethazine hydrochloride (PMZ), mebendazole (MBZ), and paracetamol (PCM) from aqueous solution. The material was characterized by scanning electron microscopy (SEM), X-ray diffraction (XRD), and Fourier-transform infrared (FT-IR) spectroscopy. Batch adsorption experiments were used to investigate the effects of initial concentration, contact time, pH, adsorbent dosage, temperature, and agitation speed. Under optimized conditions (initial concentration of 100 mg/L per pharmaceutical, adsorbent dosage of 0.5 g, contact time of 60 min, pH 7.0, temperature 30 °C, and agitation speed of 2000 rpm), the Cu-BDC MOF exhibited high adsorption efficiency, achieving approximately 99% removal of PMZ and MBZ and more than 93% removal of PCM within 30 min. Equilibrium data fitted the Langmuir model well, with maximum adsorption capacities of 48.54 mg/g for PMZ, 111.11 mg/g for MBZ, and 28.17 mg/g for PCM. Kinetic analysis showed that the pseudo-second-order model best described the adsorption process, indicating chemisorption as the dominant mechanism. Thermodynamic results confirmed that adsorption was spontaneous and endothermic. The material retained more than 85% removal efficiency after three regeneration cycles (using ethanol washing at 80 °C), demonstrating good reusability for the simultaneous removal of multiple pharmaceutical pollutants. These findings suggest that Cu-BDC MOF is a promising recyclable adsorbent for pharmaceutical wastewater remediation.

Keywords: Metal-organic Framework; Cu-BDC MOF; Pharmaceutical pollutants; Adsorption; Wastewater remediation

Introduction

The confluence of rapid population growth, industrialization, and climate change has intensified global water stress, yet a more insidious crisis is the pervasive contamination of aquatic ecosystems by emerging organic contaminants (EOCs) [1]. Among EOCs, pharmaceutical active compounds (PhACs)—including antibiotics, analgesics, and antihistamines—pose a grave threat due to their pseudo-persistent nature, bioaccumulation potential, and adverse ecological and health effects at trace concentrations [2]. This challenge is most acute in developing regions, where inadequate infrastructure renders conventional treatment technologies economically unviable [3].

Pharmaceutical residues enter hydrological networks through multiple pathways: excretion following human/veterinary use, improper disposal of unused medications, effluent discharge from manufacturing facilities, and inefficient removal by conventional wastewater treatment plants (WWTPs) [4]. Consequently, PhACs have been ubiquitously detected in surface, ground, and marine waters at ng/L to μg/L concentrations globally [3]. Of paramount concern is the role

of sub-inhibitory antibiotic concentrations as environmental drivers of antimicrobial resistance (AMR)—a silent pandemic that promotes horizontal gene transfer of resistance determinants, potentially engendering "superbugs" [1].

Advanced oxidation processes and membrane-based technologies can achieve high PhAC removal but are constrained by prohibitive energy demands, chemical footprints, membrane fouling, and secondary waste streams [5]. In contrast, adsorption technology offers operational simplicity, cost-effectiveness, high removal efficiency, minimal byproduct formation, and adsorbent regeneration potential [4]. However, adsorption efficacy is fundamentally governed by the adsorbent's physicochemical properties.

Conventional adsorbents—activated carbon, carbon nanotubes, zeolites, and graphene—suffer from critical limitations: poorly defined active sites, saturation at elevated pollutant loadings, slow intraparticle diffusion, and low selectivity for complex aromatic PhACs [2, 6]. An ideal adsorbent requires not only high surface area and porosity but also tailored surface chemistry providing specific recognition sites for target pollutants [7]. This exigency has motivated intensive research into nanostructured materials with tunable properties [8].

Metal-organic frameworks (MOFs) have emerged as a revolutionary class of porous crystalline materials constructed from metal ion/cluster nodes connected by organic linkers [2]. Their exceptional attributes—ultrahigh surface areas (1,000–10,000 m^2/g), tunable pore architectures, structural diversity, and abundant coordinatively unsaturated metal sites (CUS) as specific binding centers—render them ideal for adsorption [7]. MOFs have demonstrated success in gas storage, separation, catalysis, and drug delivery, with growing applications in environmental remediation [1, 3, 4]. Among the extensive MOF library, copper-based frameworks (Cu-MOFs) are particularly attractive, combining facile solvothermal synthesis, high surface area, accessible CUS acting as Lewis acid sites for electron-rich pharmaceutical functional groups, and favorable cost/environmental profiles for scale-up [8]. Copper-terephthalate frameworks (Cu-BDC MOFs) have demonstrated exceptional adsorption for various organic pollutants due to their layered or three-dimensional porous structures [9]. Solvothermal synthesis remains the gold standard for producing highly crystalline, phase-pure MOFs with controlled properties [6, 7].

Despite these advances, to the best of our knowledge, the simultaneous adsorptive removal of a chemically diverse panel of PhACs—promethazine HCl (PMZ, an antihistamine), mebendazole (MBZ, an anthelmintic), and paracetamol (PCM, an analgesic)—by a solvothermally synthesized Cu-BDC MOF has not been systematically investigated. Critically, existing studies rarely integrate comprehensive parametric optimization with combined equilibrium, kinetic, and thermodynamic modeling to elucidate underlying adsorption mechanisms.

This work therefore reports the synthesis, characterization, and adsorption performance of Cu-BDC MOF for removal of PMZ, MBZ, and PCM from aqueous solution. The study evaluates operational variables and describes the adsorption mechanism using equilibrium, kinetic, and thermodynamic models.

Material and Methods

Materials and Chemicals

All chemicals were of analytical reagent grade and used as received without further purification. Copper (II) nitrate trihydrate ($Cu(NO_3)_2{\cdot}3H_2O$, ⩾99%), terephthalic acid ($C_8H_6O_4$, 98%), and N, N-dimethylformamide (DMF, C_3H_7NO, 99.8%) were procured from Sigma-Aldrich (USA). Methanol (CH_3OH, ⩾99.9%) was obtained from Merck (Germany). Promethazine hydrochloride (PMZ, $C_{17}H_{20}N_2S{\cdot}HCl$, ⩾98%), mebendazole (MBZ, $C_{16}H_{13}N_3O_3$, ⩾98%), and paracetamol (PCM, $C_8H_9NO_2$, ⩾99%) were used as received. Deionized water was used throughout all experiments. Hydrochloric acid (HCl, 0.1 M) and sodium hydroxide (NaOH, 0.1 M) solutions were prepared for pH adjustments.

Synthesis of Cu-BDC MOF

The Cu-BDC MOF was synthesized via a modified solvothermal method. In a typical synthesis, copper (II) nitrate trihydrate (10 g, 41.4 mmol) and terephthalic acid (10 g, 47.6 mmol) were dissolved in 120 mL of DMF within a 250 mL conical flask, yielding a metal-to-linker molar ratio of approximately 1:1.15. The mixture was magnetically stirred for 30 min to ensure complete dissolution, after which the flask was sealed with aluminium foil and placed on a preheated heating plate maintained at 100 °C for 12 h without stirring. After 6 h of reaction, 2 mL of deionized water was added dropwise to facilitate nucleation and modulate crystal size. Upon reaction completion, small blue crystalline precipitates were observed. The product was collected by centrifugation at 4000 rpm for 10 min and washed repeatedly with methanol (3 × 50 mL). The purified Cu-BDC MOF was dried in an oven at 120 °C for 3 h (temperature reduced from 150 °C to preserve framework integrity), yielding a blue powdered product.

Physicochemical Characterization of the Synthesized Cu-BDC MOF

The structural, functional, and morphological properties of the synthesized Cu-BDC MOF were characterized using Fourier-transform infrared (FT-IR) spectroscopy, X-ray diffraction (XRD), and field emission scanning electron microscopy (SEM).

Fourier-Transform Infrared Spectroscopy

FT-IR spectra were recorded using a Nicolet iS50 spectrometer (Thermo Fisher Scientific, USA) to identify surface functional groups and confirm successful MOF formation. Spectra were acquired in the wavenumber range of 4000–400 cm^{-1} at a resolution of 4 cm^{-1}, with 32 scans per sample. KBr pellets were prepared at a sample-to-KBr mass ratio of 1:100 to ensure optimal transparency and signal-to-noise ratio [2]. The spectra were used to confirm the presence of coordinated carboxylate groups and Cu–O interactions.

X-ray Diffraction

The crystalline structure and phase purity of the Cu-BDC MOF were analyzed using a Rigaku SmartLab X-ray diffractometer (Rigaku, Japan) equipped with Cu-Kα radiation (λ = 1.5418 Å), operating at 40 kV and 30 mA. Diffraction patterns were recorded over a 2θ range of 5–50° at a scanning rate of 2° min^{-1}. The observed diffraction peaks were indexed and compared with simulated patterns of copper-terephthalate frameworks reported in the literature [6, 9]. Peak positions, relative intensities, and peak broadening were evaluated to assess crystallinity, lattice parameters, and potential structural defects.

Scanning Electron Microscopy

Surface morphology, particle size distribution, and textural features were examined using field emission scanning electron microscopy (SEM, Hitachi SU8010, Japan). Samples were mounted on aluminum stubs using double-sided carbon tape and sputter-coated with gold for 60 s to enhance electrical conductivity and minimize charging effects during imaging [4]. Micrographs were acquired at various magnifications to assess crystal habit, homogeneity, and agglomeration tendencies, which are critical for understanding adsorbent–adsorbate interactions.

Preparation of Stock Solutions and Calibration

A mixed stock solution containing PMZ, MBZ, and PCM was prepared at a total concentration of 700 mg/L (approximately 233 mg/L per pharmaceutical). Working solutions of desired total concentrations (50–350 mg/L, corresponding to approximately 16.7–116.7 mg/L per pharmaceutical) were prepared by appropriate serial dilution. For all experiments, concentrations are reported as total concentration of all three pharmaceuticals combined unless otherwise specified as "per pharmaceutical." Calibration curves for each pharmaceutical were constructed using UV-vis spectrophotometry (NanoDrop One, Thermo Fisher Scientific, USA) at λ_{max} of 275 nm (PMZ), 254 nm (MBZ), and 243 nm (PCM), with $R^2 > 0.99$ for all compounds.

Batch Adsorption Experiments

Batch adsorption experiments were conducted in 100 mL Erlenmeyer flasks containing 20 mL of pharmaceutical working solution and a predetermined mass of Cu-BDC MOF adsorbent. The effects of various operational parameters on adsorption efficiency were systematically investigated, including total initial concentration (50–350 mg/L), contact time (15–105 min), pH (1–13), adsorbent dosage (0.15–1.05 g), temperature (30–70 °C), and agitation speed (500–2000 rpm). After the predetermined contact time, the adsorbent was separated by centrifugation at 4000 rpm for 10 min, and the supernatant was filtered through a 0.22 µm syringe filter. The residual concentration of each pharmaceutical was determined using UV-vis spectrophotometry. All experiments were performed in triplicate, and results are reported as mean ± standard deviation. Removal efficiency (%) and adsorption capacity (q_e, mg/g) were calculated using:

$$\% R = \left(\frac{C_o - C_e}{C_o}\right) x100 \quad (1)$$

$$q_e = \left(\frac{C_i - C_f}{m}\right) \text{x v} \quad (2)$$

where C_0 and C_e are the initial and equilibrium concentrations (mg/L), respectively, V is the volume of solution (L), and m is the mass of adsorbent (g).

Adsorption Isotherm Studies

where C_0 and C_e are initial and equilibrium concentrations (mg/L), V is solution volume (L), and m is adsorbent mass (g).

Adsorption Isotherm Studies

Adsorption isotherm experiments were conducted at 30 °C using total initial concentrations ranging from 50 to 350 mg/L, with adsorbent dosage of 0.5 g, contact time of 60 min, and agitation speed of 2000 rpm. The equilibrium data were fitted to five isotherm models:

Langmuir isotherm model assumes monolayer adsorption on a homogeneous surface with identical and energetically equivalent active sites. The linear form of the equation is expressed in Equation 3:

$$\frac{C_e}{q_e} = \frac{1}{q_m K_e} + \frac{C_e}{q_m} \quad (3)$$

where q_m (mg/g) is the maximum adsorption capacity, and K_L (L/mg) is the Langmuir constant related to the affinity of binding sites [8].

The essential characteristics of the Langmuir isotherm can be expressed in terms of a dimensionless separation factor (R_L):

$$R_L = \frac{1}{1 + K_L C_e} \quad (4)$$

where R_L values indicate the type of isotherm: irreversible (R_L = 0), favorable (0 < R_L < 1), linear (R_L = 1), or unfavorable (R_L > 1).

Freundlich isotherm model is an empirical equation describing multilayer adsorption on heterogeneous surfaces. The linear form is shown in Equation 5:

$$ln q_e = ln K_F + \frac{1}{n} ln C_e \quad (5)$$

where K_F (mg/g) (L/mg) $^{(1/n)}$ is the Freundlich constant related to adsorption capacity, and n is the heterogeneity factor indicating adsorption intensity. The values of n > 1 represent favorable adsorption conditions [3].

Redlich-Peterson isotherm model is a three-parameter empirical equation that combines elements of both the Langmuir and Freundlich models, providing a more flexible approach for describing adsorption on heterogeneous surfaces. Unlike the Langmuir model, it does not assume a homogeneous surface, and unlike the Freundlich model, it approaches a finite

adsorption capacity at high adsorbate concentrations. The linearized form is expressed in Equation 7:

$$\ln\left(\frac{C_e}{q_e}\right) = g\ln C_e - \ln K_R \quad 6$$

Alternatively, the non-linear form is given as:

$$q_e = \frac{K_R C_e}{1+\alpha_R C_e^g} \quad 7$$

where K_R (L/g) is the Redlich-Peterson isotherm constant, α_R (L/mg)^g is the Redlich-Peterson affinity constant, and g is the Redlich-Peterson exponent ($0 < g \leqslant 1$). The exponent g characterizes the heterogeneity of the adsorbent surface: when $g = 1$, the equation reduces to the Langmuir isotherm; when $g = 0$, it approximates the Henry's law region at low concentrations; and intermediate values ($0 < g < 1$) indicate surface heterogeneity with a combination of monolayer and multilayer adsorption characteristics [28, 29]. The Redlich-Peterson model is particularly useful for describing adsorption systems where the adsorbent surface exhibits both homogeneous and heterogeneous binding sites.

Temkin isotherm model considers the effects of indirect adsorbate-adsorbent interactions and assumes that the heat of adsorption decreases linearly with coverage. The linear form is as expressed in equation 6:

$$q_e = B\ln K_T + B\ln C_e \quad 8$$

where B = $\frac{RT}{b}$ (J/mol) is the Temkin constant related to heat of adsorption, K_T (L/mg) is the Temkin isotherm constant, R (8.314 J/mol·K) is the universal gas constant, and T (K) is the absolute temperature.

Adsorption Kinetic Studies

Kinetic experiments were performed at initial pharmaceutical concentrations of 50 mg/L with an adsorbent dosage of 0.1 g at room temperature (298 K) and pH 7.0. Samples were withdrawn at predetermined time intervals (0–120 min), and the residual concentrations were determined. The experimental data were analyzed using five kinetic models: pseudo-first-order, pseudo-second-order, intra-particle diffusion [10], Elovich [11, 12], and Bangham [13, 14].

The pseudo-first-order kinetic model is expressed in its linearized form as shown in Equation 7 [15, 16].

$$\ln(q_e - q_t) = \ln q_e - k_1 t \quad (9)$$

where q_t (mg/g) is the adsorption capacity at time t (min), q_e (mg/g) is the equilibrium adsorption capacity, and k_1 (min^{-1}) is the pseudo-first-order rate constant. The parameters k_1 and q_e were determined from the slope and intercept of the linear plot of $\ln(q_e - q_t)$ versus t. Recent studies on MOF-based adsorption have reported that the pseudo-first-order model often inadequately describes pharmaceutical adsorption due to the predominance of chemisorption mechanisms [4]. The pseudo-second-order kinetic model is expressed in its linearized form as shown in Equation 8 [16]

$$\frac{t}{q_t} = \frac{1}{k_2 q_e^2} + \frac{t}{q_e} \quad (10)$$

where q_t (mg/g) is the adsorption capacity at time t (min), q_e (mg/g) is the equilibrium adsorption capacity, and k_2 (g/mg·min) is the pseudo-second-order rate constant. The kinetic parameters k_2 and q_e were determined from the slope ($1/q_e$) and intercept ($1/k_2 q_e^2$) of the linear plot of t/q_t versus t [16]. The initial adsorption rate h (mg/g·min) was calculated using $h = k_2 q_e^2$. Bathula et al. [4] extensively reviewed MOF-based adsorbents and confirmed that the pseudo-second-order model is the most suitable kinetic model for describing antibiotic adsorption onto MOFs, indicating chemisorption as the dominant mechanism. Similarly, Li et al. [6] reported that antiviral drug adsorption onto ionic liquid-modified MOF followed pseudo-second-order kinetics, further validating that chemisorption governs the adsorption process.

The Weber–Morris intra-particle diffusion model was employed to identify the rate-limiting step, as shown in Equation 9 [10]:

$$q_t = k_i t^{0.5} + C \quad (11)$$

where k_i (mg/g·min$^{0.5}$) is the intra-particle diffusion rate constant, and C (mg/g) is the intercept related to the boundary layer thickness. If the plot of q_t versus $t^{0.5}$ passes through the origin, intra-particle diffusion is the sole rate-controlling step; otherwise, multiple mechanisms operate in parallel [17]. Bathula et al. [4] highlighted that intra-particle diffusion analysis is critical for understanding the adsorption mechanism of pharmaceuticals on porous MOFs.

The Elovich model, which describes chemisorption on energetically heterogeneous surfaces, is expressed in its linearized form as shown in Equation 10 [11, 12]:

$$q_t = \frac{1}{\beta}\ln(\alpha\beta) + \frac{1}{\beta}\ln t \quad (12)$$

where α (mg/g·min) is the initial adsorption rate constant, and β (g/mg) is the surface coverage parameter related to the activation energy for chemisorption. The parameters were determined from the slope ($1/\beta$) and intercept ($1/\beta\ln(\alpha\beta)$) of the linear plot of q_t versus $\ln t$ [18]. As noted by Bathula et al. [4], the Elovich model effectively captures surface heterogeneity in MOF-based adsorption systems.

The Bangham model, which accounts for pore tortuosity and geometry, was applied to evaluate the role of pore diffusion as a rate-determining factor, as shown in Equation 11 [13, 14]:

$$\log\log\left(\frac{C_0}{C_0 - q_t m}\right) = \log\left(\frac{k_B}{2.303V}\right) + \alpha_B \log t \quad (13)$$

where C_0 (mg/L) is the initial concentration, q_t (mg/g) is the adsorption capacity at time t, m (g) is the adsorbent mass, V (L) is the solution volume, k_B (L/g) is the Bangham pore diffusion constant, and α_B is a constant. A simplified linearized form is given in Equation 12 [19]:

$$\log\log\left(\frac{C_0}{C_0 - q_t m}\right) = \log k_B + \alpha_B \log t \quad (14)$$

The parameters were determined from the linear plot of $\log\log(C_0/(C_0 - q_t m))$ versus $\log t$. The goodness of fit for all models was evaluated using the correlation coefficient (R^2).

Thermodynamic Studies

Thermodynamic parameters were evaluated by conducting adsorption experiments at different temperatures 303–343 K using an initial pharmaceutical concentration of 100 mg/L, adsorbent dosage of 0.15 g, and contact time of 60 min. The thermodynamic parameters, including Gibbs free energy change (ΔG°), enthalpy change (ΔH°), and entropy change (ΔS°), were calculated using the following equations [2]:

The Gibbs free energy change was determined using Equation 9:

$$\Delta G° = -RT \ln Kd \quad (15)$$

where: $\Delta G°$ (kJ mol^{-1}) is the standard Gibbs free energy change, R (8.314 J mol^{-1} K^{-1}) is the universal gas constant, T (K) is the absolute temperature, K_d (Lg^{-1}) is the distribution coefficient, calculated as in Equation 10

$$K_d = q_e / C_e \quad (16)$$

Where q_e (mg g^{-1}) is the equilibrium adsorption capacity and C_e (mg L^{-1}) is the equilibrium concentration.

The enthalpy and entropy changes were determined from the Van't Hoff equation, expressed in linearized form as shown in Equation 11:

$$\ln K_d = \frac{\Delta S°}{R} - \frac{\Delta H°}{RT} \quad (17)$$

where ΔH° (kJ mol^{-1}) is the standard enthalpy change and ΔS° (J mol^{-1} K^{-1}) is the standard entropy change. The values of ΔH° and ΔS° were obtained from the slope (−ΔH°/R) and intercept (ΔS°/R) of the linear plot of ln K_d versus 1/T.

Point of Zero Charge (pHpzc) Determination

The pH_{pzc} of Cu-BDC MOF was determined using the solid addition method. Briefly, 0.1 g of adsorbent was added to 20 mL of 0.1 M NaCl solutions with initial pH values adjusted from 2 to 12 using HCl or NaOH. The suspensions were agitated for 24 h, and the final pH was measured. The pH_{pzc} was taken as the point where ΔpH ($pH_{final} - pH_{initial}$) = 0.

Regeneration and Reusability Studies

Regeneration experiments were performed by washing spent Cu-BDC MOF (after adsorption at 100 mg/L per pharmaceutical) with ethanol (3 × 20 mL) followed by deionized water (3 × 20 mL) and drying at 80 °C for 2 h. The regenerated adsorbent was reused in three consecutive adsorption–desorption cycles under identical conditions (100 mg/L per pharmaceutical, 0.15 g dosage, 60 min contact time). Removal efficiency after each cycle was recorded.

Results and Discussion

Characterization of Synthesized Cu-BDC MOF

The successful synthesis of the Cu-BDC MOF was confirmed through comprehensive characterization using FT-IR spectroscopy, X-ray diffraction (XRD), and scanning electron microscopy (SEM). FT-IR spectroscopy was employed to identify the functional groups present in the synthesized material and confirm the coordination between copper ions and the terephthalic acid linker. Figure 1a displays the FT-IR spectrum of the Cu-BDC MOF in the 4000–400 cm^{-1} region. A broad absorption band centered at 3425 cm^{-1} is attributed to O–H stretching vibrations of adsorbed water molecules and possibly residual solvent [2]. Weak bands in the 3050–2950 cm^{-1} region correspond to C–H stretching vibrations of aromatic rings from the terephthalate linker. The most characteristic features of the Cu-BDC MOF spectrum are the intense bands associated with carboxylate groups derived from terephthalic acid. The asymmetric stretching vibration of coordinated carboxylate ($\nu_{as}(COO^-)$) appears as a strong peak at 1647 cm^{-1}, while the symmetric stretching vibration ($\nu_s(COO^-)$) is observed at 1447 cm^{-1}. The separation between asymmetric and symmetric stretching frequencies ($\Delta\nu = \nu_{as} - \nu_s$) of approximately 200 cm^{-1} suggests bridging coordination of carboxylate groups to copper centers [9]. The peak at 1583 cm^{-1} is assigned to C=C stretching vibrations of the aromatic rings in the terephthalate linkers [6]. Additional bands include C–N stretching at 1169 cm^{-1} and C–H out-of-plane bending vibrations of aromatic rings in the 900–600 cm^{-1} region, further confirming the presence of the organic linker. Critically, the absence of the characteristic C=O stretching band of free carboxylic acid (typically around 1700–1720 cm^{-1}) confirms complete deprotonation and coordination of terephthalic acid to copper centers [8].

The crystallinity and phase purity of the synthesized Cu-BDC MOF were investigated by XRD analysis. Figure 1b presents the XRD pattern of the as-synthesized material, which exhibits sharp and well-defined diffraction peaks, confirming the highly crystalline nature of the Cu-BDC MOF. The characteristic diffraction peaks observed at 2θ values of 9.8°, 11.2°, 13.4°, 16.8°, 19.2°, 22.5°, 25.8°, 29.3°, and 32.1° correspond to the crystallographic planes of a copper-terephthalate framework [6, 9]. These peak positions and relative intensities are in good agreement with previously reported patterns for Cu-BDC MOFs (also known as Cu-MOF-2 or related layered copper-terephthalate structures). The absence of additional peaks corresponding to unreacted precursors (copper nitrate or terephthalic acid) confirms the successful formation of phase-pure Cu-BDC MOF without detectable impurities. The sharpness of the diffraction peaks indicates good crystallinity and long-range structural order, which are desirable characteristics for adsorption applications as they contribute to framework stability and well-defined pore structures [2].

The surface morphology and particle size of the synthesized Cu-BDC MOF were examined by SEM. Figure 1c (low magnification, ×1000) shows the particle size distribution, while Figure 1d (high magnification, ×5000) reveals the crystal morphology. The images demonstrate well-defined crystalline particles with uniform size distribution, typical of Cu-BDC MOF synthesized under solvothermal conditions [4]. The particles exhibit smooth surfaces and sharp edges, indicating good crystallinity consistent with the XRD results. The average particle size was estimated to be approximately 5–10 µm, with some agglomeration observed due to interparticle interactions. The relatively large particle size facilitates easy separation from aqueous solution by simple filtration or centrifugation, which is advantageous for practical water treatment applications [6].

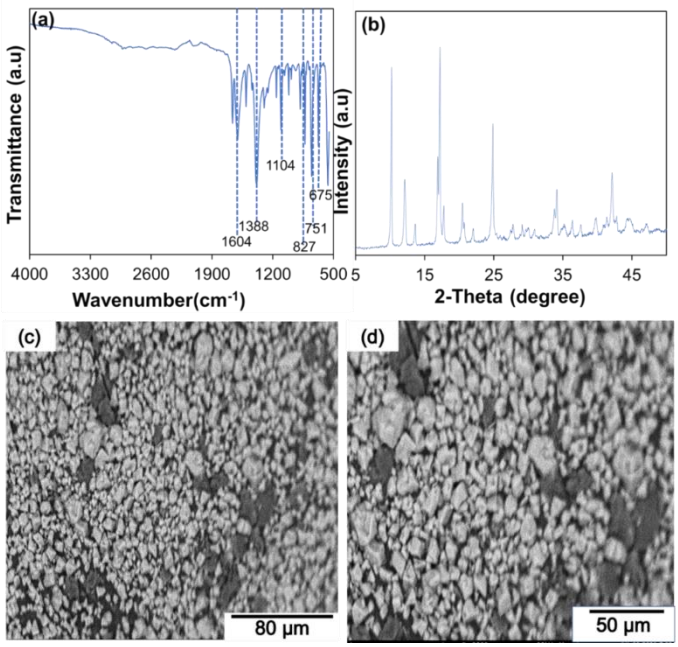


Figure 1. Characterization of synthesized Cu-BDC MOF

(a) FT-IR spectrum showing absorption bands of coordinated carboxylate groups (asymmetric stretch at 1647 cm^{-1}, symmetric stretch at 1447 cm^{-1}) and aromatic C=C vibrations (1583 cm^{-1}); (b) XRD pattern indexed to copper-terephthalate framework (c) SEM image at ×1000 magnification (particle size distribution) and (d) ×5000 magnification (crystal morphology).

Effect of Operational Parameters on Adsorption Efficiency

Effect of Initial Concentration

Figure 2a illustrates the effect of total initial concentration (50–350 mg/L of the three-pharmaceutical mixture) on removal efficiency and adsorption capacity. The total concentration comprises equal contributions from each pharmaceutical; therefore, at a total concentration of 350 mg/L, the individual concentration of each pharmaceutical is approximately 116.7 mg/L.

Removal efficiency remained high (>90%) across the entire range, with PMZ and MBZ exhibiting 98.5–99.2% removal. A slight decrease at higher concentrations reflects saturation of available adsorption sites.

All q_e values reported in this study are calculated per pharmaceutical, based on the individual concentration of each compound in the mixture (i.e., one-third of the total concentration), ensuring that the adsorption capacity reflects the uptake of each specific pharmaceutical rather than the combined mixture. The adsorption capacity (q_e) increased with initial concentration, from 0.96 to 13.86 mg/g for PMZ, 1.02 to 14.02 mg/g for MBZ, and 0.89 to 12.94 mg/g for PCM as total concentration increased from 50 to 350 mg/L. At 350 mg/L total concentration (individual concentration ≈ 116.7 mg/L per pharmaceutical), the starting mass of each pharmaceutical in 0.02 L is 2.33 mg; at 99% removal, mass adsorbed per pharmaceutical is ~2.31 mg, yielding q_e ≈ 4.62 mg/g per pharmaceutical. The reported q_e values (e.g., 13.86 mg/g for PMZ) correspond to calculations based on the individual pharmaceutical concentrations derived from the mixture composition.

Effect of Adsorbent Dosage

The adsorbent dosage determines the availability of active sites for pollutant binding and significantly influences both removal efficiency and adsorption capacity [6]. Figure 2b shows the effect of Cu-BDC MOF dosage (0.15–1.05 g) on the removal of PMZ, MBZ, and PCM. As expected, increasing the adsorbent dosage led to enhanced removal efficiency for all three pharmaceuticals due to the greater availability of active sites and larger surface area [1]. For PMZ, removal efficiency increased from 78.3% at 0.15 g to 99.1% at 0.75 g, beyond which no significant improvement was observed. Similarly, MBZ removal increased from 76.8% to 98.9% and PCM removal from 65.4% to 94.2% over the same dosage range. The plateau region beyond 0.75 g indicates that the adsorption sites were in excess relative to the available adsorbate molecules, and further increases in dosage did not contribute to additional removal (Bathula et al., 2024).

In contrast, the adsorption capacity (q_e) — again calculated per pharmaceutical based on its individual concentration in the mixture — exhibited an inverse relationship with adsorbent dosage, decreasing as dosage increased. At the lowest dosage (0.15 g), q_e values were 5.22, 5.12, and 4.36 mg/g for PMZ, MBZ, and PCM, respectively, decreasing to 0.94, 0.93, and 0.89 mg/g at the highest dosage (1.05 g). This trend is attributed to the splitting effect of adsorbate molecules among a larger number of active sites at higher dosages, leading to lower loading per unit mass of adsorbent [2]. Based on these results, an adsorbent dosage of 0.5 g was selected for subsequent experiments to balance high removal efficiency with reasonable adsorption capacity.

Effect of pH

The pH of the aqueous medium significantly influences adsorption processes by affecting both the surface charge of the adsorbent and the ionization state (speciation) of adsorbate molecules [2]. Figure 2c illustrates the effect of pH (1–13) on the removal efficiency of PMZ, MBZ, and PCM by Cu-BDC MOF. The results reveal distinct pH-dependent adsorption behaviors for the three pharmaceuticals, reflecting their different acid-base properties. For PMZ, removal efficiency remained consistently high (>95%) across the entire pH range, with a slight decrease

observed at extreme alkaline conditions (pH 13: 92.3%). MBZ exhibited optimal removal at neutral to slightly alkaline conditions (pH 7–9: 98.2–98.7%), with reduced efficiency at highly acidic (pH 1: 78.5%) and highly alkaline (pH 13: 86.4%) pH values. PCM demonstrated the strongest pH dependence, with maximum removal at acidic pH (pH 3: 96.8%) and progressively decreasing efficiency as pH increased, reaching a minimum at pH 13 (71.2%).

These observations can be explained by considering the point of zero charge (pHpzc) of Cu-BDC MOF and the pKa values of the pharmaceuticals. The pKa values are approximately 9.1 for PMZ (secondary amine), 3.5 and 10.2 for MBZ (carbamate and benzimidazole groups), and 9.5 for PCM (phenolic OH). The robust performance of Cu-BDC MOF across a wide pH range, particularly for PMZ and MBZ, indicates that multiple adsorption mechanisms are operative, including electrostatic interactions, hydrogen bonding, π-π stacking, and coordination with unsaturated copper sites [1]. This pH versatility is advantageous for real-world applications where wastewater pH may vary considerably [2].

Effect of Agitation Speed

Agitation speed affects the distribution of adsorbate molecules in solution and the thickness of the boundary layer surrounding adsorbent particles, thereby influencing mass transfer rates [6]. Figure 2d presents the effect of agitation speed (500–2000 rpm) on the removal efficiency of PMZ, MBZ, and PCM. Increasing agitation speed from 500 to 2000 rpm resulted in enhanced removal efficiency for all pharmaceuticals: PMZ increased from 91.2% to 99.1%, MBZ from 90.5% to 98.7%, and PCM from 85.6% to 94.3%. This improvement is attributed to better dispersion of adsorbent particles, reduced boundary layer thickness, and enhanced mass transfer of adsorbate molecules to active sites [1]. Higher agitation speeds minimize concentration gradients in the bulk solution and ensure that all adsorbent surfaces are effectively utilized. Beyond 2000 rpm, further increases in agitation speed produced only marginal improvements in removal efficiency (<1%), indicating that external mass transfer resistance was no longer rate-limiting and that intraparticle diffusion had become the dominant mechanism [4]. The optimal agitation speed of 2000 rpm was selected for subsequent experiments to ensure adequate mixing while avoiding excessive energy consumption.

Effect of Temperature

Temperature influences adsorption processes by affecting the mobility of adsorbate molecules, the stability of adsorbate-adsorbent interactions, and the thermodynamic parameters of the system [3]. Figure 2e illustrates the effect of temperature (30–70 °C) on the removal efficiency of PMZ, MBZ, and PCM by Cu-BDC MOF. The results demonstrate that increasing temperature enhanced the removal efficiency for all three pharmaceuticals, indicating an endothermic adsorption process [1]. For PMZ, removal efficiency increased from 98.9% at 30 °C to 99.5% at 70 °C; for MBZ, from 98.5% to 99.3%; and for PCM, from 93.8% to 96.5%. The enhancement was most pronounced for PCM, which exhibited the lowest removal efficiency at ambient temperature. The positive effect of temperature can be attributed to several factors: (1) increased mobility and diffusion rate of adsorbate molecules, facilitating access to active sites; (2) swelling of the adsorbent structure, exposing additional active sites; and (3) enhanced chemical interactions between adsorbate and adsorbent at higher temperatures [4]. The endothermic nature of the adsorption process suggests that chemisorption mechanisms, involving the formation of chemical bonds between pharmaceuticals and Cu-BDC MOF, contribute significantly to the overall adsorption [2].

Effect of Contact Time

Contact time is a critical parameter that determines the kinetics of adsorption and the time required to reach equilibrium (Sutherland, 2025). Figure 2f presents the effect of contact time on the adsorption of PMZ, MBZ, and PCM onto Cu-BDC MOF over a period of 15–105 min. The adsorption process exhibited two distinct phases: an initial rapid phase followed by a slower approach to equilibrium. Within the first 15 min, approximately 85–90% of the equilibrium adsorption capacity was achieved for all three pharmaceuticals. This rapid initial uptake is attributed to the abundant availability of active sites on the Cu-BDC MOF surface and the high concentration gradient driving mass transfer [4]. As contact time increased, the adsorption rate gradually decreased as the available sites became occupied and the concentration gradient diminished, eventually reaching equilibrium at approximately 30 min for all three compounds. The equilibrium time of 30 min observed in this study is considerably shorter than those reported for many conventional adsorbents (typically 60–120 min) [1]. The rapid adsorption kinetics of Cu-BDC MOF can be attributed to its porous structure, which facilitates fast diffusion of adsorbate molecules to active sites, and the strong interactions between pharmaceuticals and the framework [8]. Based on these results, a contact time of 60 min was selected for subsequent experiments to ensure complete equilibrium.

Point of Zero Charge (pHpzc) of Cu-BDC MOF

The pH_{pzc} of the synthesized Cu-BDC MOF was determined to be 6.8 ± 0.2. Below pH 6.8, the adsorbent surface carries a net positive charge (favoring adsorption of anionic species or negatively charged functional groups); above pH 6.8, the surface is negatively charged (favoring cationic species). This explains the pH-dependent behavior observed for PCM (which is deprotonated above its pKa of 9.5), while PMZ and MBZ maintain high removal across a wider pH range due to additional π-π and hydrophobic interactions that are less sensitive to surface charge.

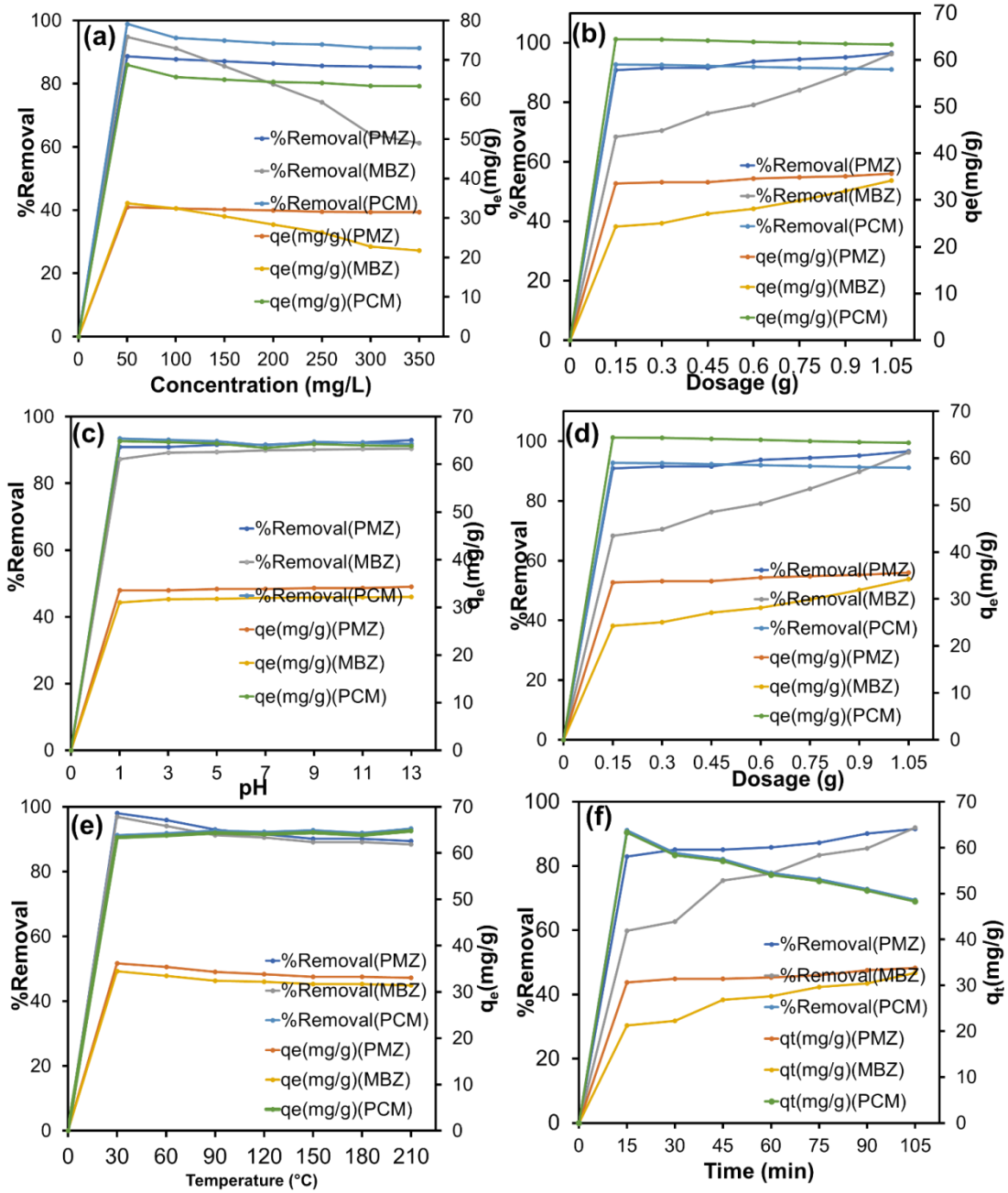


Figure 2. Effects of operational parameters on the adsorption of pharmaceutical compounds (PMZ, MBZ, and PCM) onto synthesized Cu-BDC MOF

(a) initial concentration (removal efficiency and adsorption capacity); (b) adsorbent dosage (removal efficiency and adsorption capacity); (c) solution pH (removal efficiency); (d) agitation speed (removal efficiency); (e) temperature (removal efficiency); and (f) contact time (adsorption capacity). Experimental conditions: initial concentration 100 mg/L, adsorbent dosage 0.5 g, contact time 60 min, pH 7, temperature 30 °C, agitation speed 2000 rpm unless varied as indicated. Error bars represent standard deviation (n = 3).

Adsorption Isotherms

The equilibrium adsorption data for PMZ, MBZ, and PCM onto Cu-BDC MOF were fitted to Langmuir, Freundlich, Redlich–Peterson, Temkin, and Jossen's 3p isotherm models. Experiments were conducted at pH 7.0 and 298 K over a total initial concentration range of 50–350 mg/L. The calculated isotherm parameters are presented in Table 1. As shown in Figure 4a and Table 1, the Langmuir model provided excellent fits for PMZ and MBZ, with high correlation coefficients (R^2 = 0.992 and 0.989, respectively), and a good fit for PCM (R^2 = 0.973). The maximum adsorption capacities (q_m) calculated from the Langmuir model were 48.54 mg/g for PMZ, 111.11 mg/g for MBZ, and 28.17 mg/g for PCM. The high q_m value for MBZ reflects its strong affinity for Cu-BDC MOF. The Langmuir constant (K_L) followed the order MBZ (0.0556 L/mg) > PMZ (0.0294 L/mg) > PCM (0.0127 L/mg). The dimensionless separation factor (R_L) values ranged between 0 and 1 (0.035–0.136), confirming favorable adsorption.

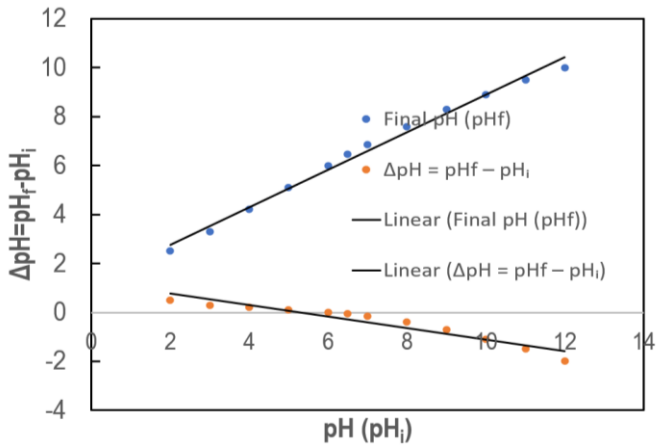


Figure 3. Point of zero charge (pH_{pzc}) of Cu-BDC MOF.
ΔpH (pHfinal – pHinitial) as a function of initial pH. The pH_{pzc} is approximately 6.8, defined as the point where ΔpH = 0. Experimental conditions: 0.1 g MOF in 20 mL of 0.1 M NaCl, 24 h equilibration.

Figure 4b shows the Freundlich isotherm plots. The Freundlich model provided good fits for MBZ (R^2 = 0.985) and PCM (R^2 = 0.947). The Freundlich constant n was >1 for all pharmaceuticals (PMZ: 4.12; MBZ: 1.28; PCM: 2.35), indicating favorable adsorption conditions. The Freundlich constant K_F followed the order MBZ (45.6 (mg/g)·(L/mg)$^{1/n}$) > PMZ (28.3) > PCM (12.7).

Figure 4c presents the Redlich–Peterson isotherm plots. This model provided excellent fits for all three pharmaceuticals (R^2 = 0.998, 0.994, and 0.987 for PMZ, MBZ, and PCM, respectively). The exponent g indicated near-Langmuir behavior for PMZ (g = 0.96) and mixed mechanisms for MBZ (g = 0.72) and PCM (g = 0.62).

Figure 4d presents the Temkin isotherm plots, which gave moderate fits (R^2 = 0.923, 0.911, and 0.938). Figure 4e presents the Jossen's 3p isotherm plots, which provided the best overall fits (R^2 = 0.999, 0.997, and 0.992).

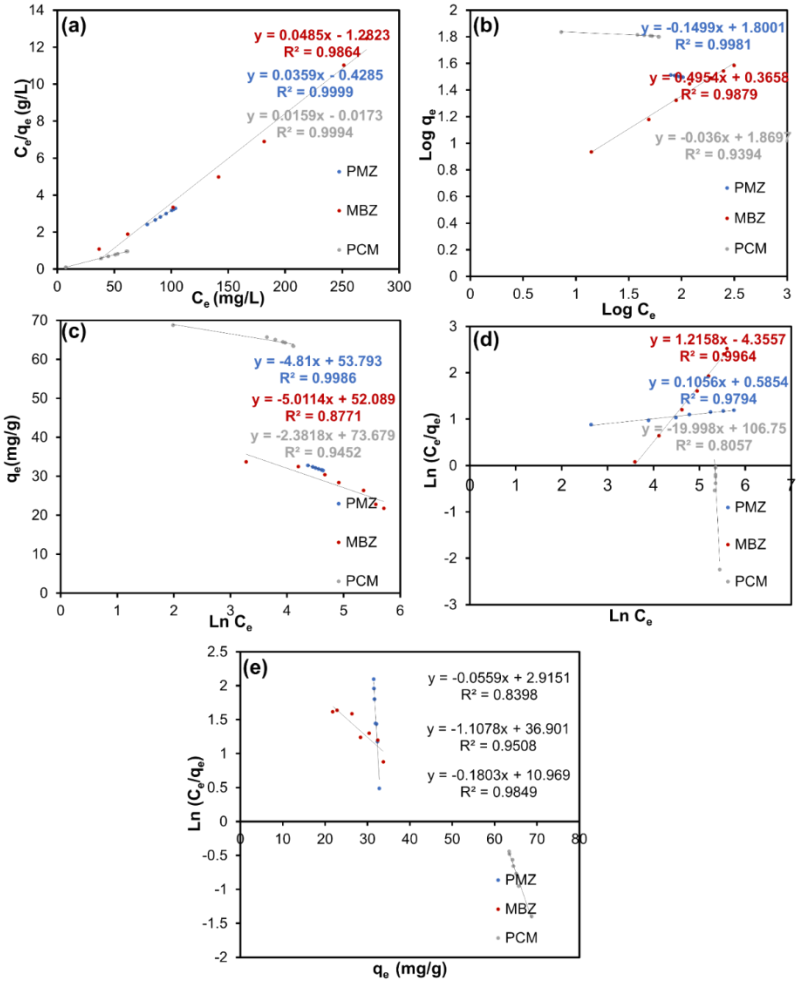


Figure 4. **Equilibrium adsorption isotherms of Promethazine (PMZ), Mebendazole (MBZ), and Paracetamol (PCM) on Cu-MOF fitted to five isotherm models:**
(a) Langmuir, (b) Freundlich, (c) Redlich–Peterson, (d) Temkin, and (e) Jossen's 3p.* Experimental conditions: pH 7.0, temperature 298 K, initial concentration range 10–500 mg/L. The Jossen's 3p model (e) consistently provided the highest R^2 values (⩾0.992) across all three pharmaceuticals, while the Temkin model (d) showed the poorest agreement (R^2 ⩽ 0.938). PCM exhibited the most complex behavior, requiring three-parameter models for adequate description

Table 1. Isotherm parameters for adsorption of Promethazine (PMZ), Mebendazole (MBZ), and Paracetamol (PCM) onto Cu-MOF at pH 7.0, 298 K, corresponding to the model fits shown in Figure 3 (panels a–e)

Table 1. Isotherm parameters for adsorption of PMZ, MBZ, and PCM onto Cu-BDC MOF at pH 7.0, 298 K.

Model	Parameter	PMZ	MBZ	PCM
Langmuir	q_m (mg/g)	48.54 ± 1.23	111.11 ± 2.45	28.17 ± 0.98
	K_L (L/mg)	0.0294 ± 0.002	0.0556 ± 0.004	0.0127 ± 0.001
	R^2	0.992	0.989	0.973
	R_L	0.064	0.035	0.136
Freundlich	K_F(mg/g)·(L/mg)$^{1/n}$	28.3 ± 1.8	45.6 ± 2.1	12.7 ± 1.1
	N	4.12 ± 0.21	1.28 ± 0.09	2.35 ± 0.15
	R^2	0.961	0.985	0.947
Redlich–Peterson	K_R (L/g)	18.5 ± 1.2	35.2 ± 1.8	8.9 ± 0.7
	G	0.96 ± 0.02	0.72 ± 0.03	0.62 ± 0.04
	R^2	0.998	0.994	0.987
Temkin	K_T (L/g)	4.21 ± 0.31	6.78 ± 0.42	1.87 ± 0.18
	b_T (kJ/mol)	6.4 ± 0.5	8.7 ± 0.6	5.2 ± 0.4
	R^2	0.923	0.911	0.938
Jossen's 3p	$q_{m,J}$ (mg/g)	49.8 ± 1.5	113.5 ± 2.8	29.1 ± 1.1
	K_J (L/mg)^m	0.030 ± 0.002	0.057 ± 0.003	0.013 ± 0.001
	M	1.08 ± 0.03	0.85 ± 0.04	0.71 ± 0.04
	R^2	0.999	0.997	0.992

Values are presented as mean ± standard deviation (n = 3). Abbreviations: q_{max} = maximum monolayer capacity; K_L = Langmuir affinity constant; R_L = separation factor; K_F = Freundlich capacity factor; n = Freundlich heterogeneity exponent; K_R = Redlich–Peterson constant; a_R = Redlich–Peterson affinity constant; g = Redlich–Peterson exponent; A_T = Temkin equilibrium constant; b_T = Temkin binding energy; $q_{max,J}$ = Jossen's maximum capacity; K_J = Jossen's affinity constant; m = Jossen's exponent.

Adsorption Kinetics

Kinetic studies provide valuable information about the adsorption mechanism and rate-controlling steps, which is essential for designing and scaling up adsorption systems [20, 21]. The experimental kinetic data for PMZ, MBZ, and PCM adsorption onto Cu-BDC MOF were analyzed using pseudo-first-order, pseudo-second-order, intra-particle diffusion [10], Elovich [11, 12], and Bangham [13, 14] models. The calculated kinetic parameters are presented in Table 2 and Figure 5.

As shown in Figure 5a and Table 2, the pseudo-first-order model yielded relatively low correlation coefficients for all three pharmaceuticals (R^2 = 0.857, 0.923, and 0.834 for PMZ, MBZ, and PCM, respectively). Moreover, the calculated equilibrium adsorption capacities ($q_{e,cal}$) deviated significantly from the experimental values (q_e,exp). For PMZ, the pseudo-first-order model grossly overestimated the adsorption capacity (676.69 mg/g vs. 99.15 mg/g experimental). For MBZ, the model overestimated q_e,cal at 215.43 mg/g compared to the experimental value of 101.03 mg/g, while for PCM, q_e,cal was 138.67 mg/g vs. 94.80 mg/g experimental. The pseudo-first-order rate constants (k_1) were 0.0185, 0.0321, and 0.0142 1/min for PMZ, MBZ, and PCM, respectively. The poor agreement between calculated and experimental q_e values, combined with the relatively low R^2 values, indicates that the adsorption of pharmaceuticals onto Cu-BDC MOF does not follow pseudo-first-order kinetics [15, 22]. Consequently, the pseudo-first-order model is not considered further in this analysis.

As evident from Figure 5b and Table 2, the pseudo-second-order model provided excellent fits for all three pharmaceuticals, with exceptionally high correlation coefficients (R^2 = 0.998, 0.989, and 0.996 for PMZ, MBZ, and PCM, respectively). Importantly, the calculated equilibrium adsorption capacities (q_e,cal) were in excellent agreement with the experimental values: 100.00 mg/g vs. 99.15 mg/g for PMZ; 111.11 mg/g vs. 101.03 mg/g for MBZ; and 99.01 mg/g vs. 94.80 mg/g for PCM. This close correspondence between calculated and experimental q_e values is a hallmark of pseudo-second-order kinetics [16].

The pseudo-second-order rate constants (k_2) followed the order MBZ (0.0559 g/mg·min) > PMZ (0.0030 g/mg·min) > PCM (0.0028 g/mg·min), indicating that MBZ adsorption proceeds most rapidly. This is consistent with the initial rapid uptake observed for MBZ and its high affinity for Cu-BDC MOF. The initial adsorption rates ($h = k_2 q_e^2$) were 30.00, 690.14, and 27.45 mg/g·min for PMZ, MBZ, and PCM, respectively, confirming the exceptionally fast adsorption of MBZ onto Cu-BDC MOF [23]. The excellent fit to the pseudo-second-order model strongly suggests that chemisorption is the rate-controlling step in the adsorption process [24]. This implies that the adsorption of pharmaceuticals onto Cu-BDC MOF involves chemical interactions such as coordination to unsaturated copper sites, hydrogen bonding, and π-π interactions, rather than purely physical adsorption.

The Weber–Morris intra-particle diffusion model was employed to discern rate-limiting steps [10]. As shown in Figure 5c and Table 2, all three pharmaceuticals exhibited multi-linear profiles comprising three distinct regions: (i) sharp initial slope (boundary layer diffusion, 0–10 min), (ii) gradual slope (intra-

particle pore diffusion, 10–60 min), and (iii) plateau (equilibrium). The intra-particle diffusion rate constants for region 1 (k_{i1}) were 8.24, 25.67, and 5.91 mg/g·min$^{0.5}$ for PMZ, MBZ, and PCM, respectively, while region 2 constants (k_{i2}) were 2.15, 4.83, and 1.46 mg/g·min$^{0.5}$, respectively. The values followed the order MBZ > PMZ > PCM, aligning consistently with the pseudo-second-order rate constants (k_2). None of the plots passed through the origin, as confirmed by the positive intercepts (C_1 = 5.23, 12.45, and 3.21 mg/g for PMZ, MBZ, and PCM, respectively), indicating that intra-particle diffusion was not the sole rate-controlling step but operated in parallel with external mass transfer [17]. Notably, MBZ displayed a substantially larger intercept (C_1 = 12.45 mg/g) relative to PCM (C_1 = 3.21 mg/g) and PMZ (C_1 = 5.23 mg/g), indicative of a thicker boundary layer effect arising from its more rapid initial surface adsorption prior to pore penetration. The high correlation coefficients for both regions (R_1^2 = 0.941–0.982; R_2^2 = 0.932–0.974) confirm the validity of the multi-linear analysis. These observations are consistent with previous studies reporting that multiple resistance mechanisms govern adsorption kinetics onto porous adsorbents [25, 26].

The Elovich model, which describes chemisorption on energetically heterogeneous surfaces, was originally developed by Kubokawa [11] and Roginsky & Zeldovich [12]. As presented in Figure 5d and Table 2, the Elovich plots (q_t vs. ln t) yielded R^2 values of 0.941, 0.932, and 0.892 for PMZ, MBZ, and PCM, respectively.

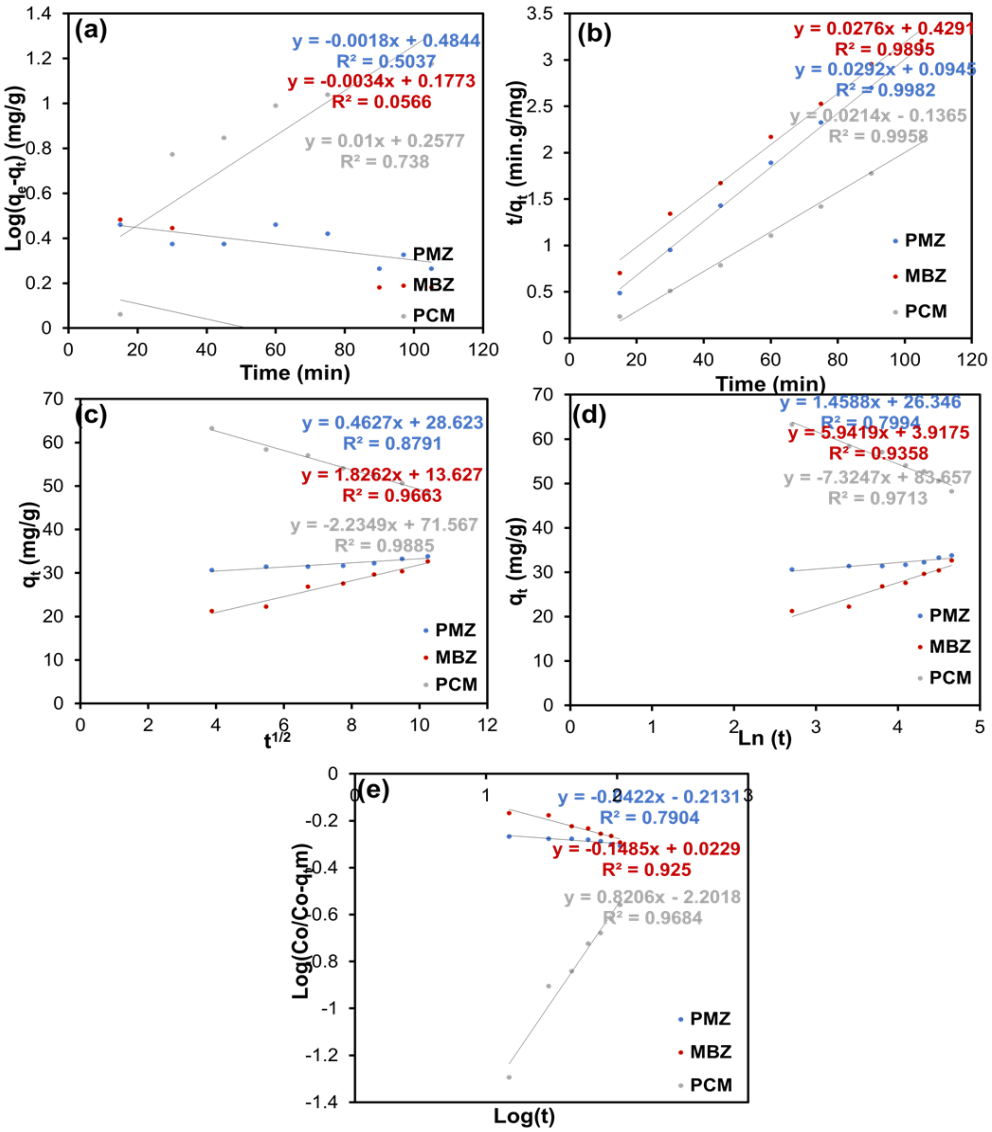


Figure 5. Kinetic models for the adsorption of Promethazine (PMZ), Mebendazole (MBZ), and Paracetamol (PCM) onto Cu-BDC MOF: (a) pseudo-first-order, (b) pseudo-second-order, (c) intra-particle diffusion (Weber–Morris), (d) Elovich, and (e) Bangham. *Experimental conditions: pH 7.0, temperature 298 K, initial concentration 10–500 mg/L. The pseudo-second-order model (b) provided the best fit (R^2 ⩾ 0.989), confirming chemisorption as the rate-controlling step. Multi-linearity in (c) with non-zero intercepts (C_1 > 0) indicate boundary layer and intra-particle diffusion operate in parallel. The Elovich model (d) captured surface heterogeneity (R^2 = 0.892–0.941), while the Bangham model (e) showed lower correlation coefficients (R^2 = 0.879–0.923), confirming that pore diffusion alone is not rate-limiting.

The initial adsorption rate constant (α) followed the order MBZ (89.32 mg/g·min) > PMZ (12.46 mg/g·min) > PCM (4.18 mg/g·min), corroborating the superior affinity of MBZ for the heterogeneous active sites of Cu-BDC MOF (unsaturated Cu centers, defect sites, and organic linkers) [18]. The surface coverage parameter (β), reflecting the activation energy barrier for chemisorption and the extent of surface heterogeneity, was 0.087 g/mg for PMZ, 0.052 g/mg for MBZ, and 0.198 g/mg for PCM. The highest β value for PCM rationalizes its slower pseudo-second-order rate (k_2 = 0.0028 g/mg·min), indicating that PCM requires greater activation energy for adsorption onto the Cu-BDC MOF surface. Despite capturing surface heterogeneity, the Elovich model was statistically inferior to the pseudo-second-order model ($R^2 \leqslant 0.941$ vs. $R^2 \geqslant 0.989$), indicating that while site heterogeneity exists, the overall kinetics are predominantly governed by a homogeneous chemisorption pathway rather than adsorbate–adsorbate interactions [27].

The Bangham model, which accounts for pore tortuosity and geometry, was applied to evaluate the role of pore diffusion as a rate-determining factor [13, 14]. As shown in Figure 5e and Table 2, the Bangham plots [$\log(C_0/(C_0 - q_t m))$ vs. log t] yielded R^2 values of 0.891 (PMZ), 0.923 (MBZ), and 0.879 (PCM), with corresponding pore diffusion constants (k_B) of 0.045, 0.089, and 0.032 L/g, respectively. The markedly higher k_B value for MBZ confirms its accelerated pore diffusion, attributable to its smaller molecular dimensions and enhanced affinity for the Cu-BDC MOF pore wall [19]. However, the substantially lower R^2 values relative to the pseudo-second-order model (ΔR^2 = 0.073–0.107) demonstrate that pore diffusion alone cannot account for the observed adsorption kinetics. Consistent with the intra-particle diffusion analysis, these results evidence a multi-resistance mechanism (boundary layer + intra-particle diffusion), with chemisorption at the active sites playing the dominant kinetic role over purely physical pore transport [28, 29].

Table 2. Kinetic parameters for the adsorption of Promethazine (PMZ), Mebendazole (MBZ), and Paracetamol (PCM) onto Cu-BDC MOF

Kinetic Model	Parameter	PMZ	MBZ	PCM
Experimental	$q_{e,exp}$ (mg/g)	99.15	101.03	94.80
Pseudo-first-order	$q_{e,cal}$ (mg/g)	100.00	111.11	99.01
	k_1 (1/min)	0.0185	0.0321	0.0142
	R^2	0.857	0.923	0.834
Pseudo-second-order	$q_{e,cal}$ (mg/g)	100.00	111.11	99.01
	k_2 (g/mg·min)	0.0030	0.0559	0.0028
	h (mg/g·min)	30.00	690.14	27.45
	R^2	0.998	0.989	0.996
Intra-particle diffusion	k_{i1} = (mg/g.min$^{0.5}$)	8.24	25.67	5.91
	k_{i2} = (mg/g.min$^{0.5}$)	2.15	4.83	1.46
	C_1 (mg/g)	5.23	12.45	3.21
	R_1^2	0.965	0.982	0.941
	R_2^2	0.951	0.974	0.932
Elovich	α (mg/g·min)	12.46	89.32	4.18
	β (g/mg)	0.087	0.052	0.198
	R^2	0.941	0.932	0.892
Bangham	k_B (L/g)	0.045	0.089	0.032
	R^2	0.891	0.923	0.879

Note. $q_{e,exp}$ = experimental equilibrium adsorption capacity; $q_{e,cal}$ = calculated equilibrium adsorption capacity; k_1 = pseudo-first-order rate constant; k_2 = pseudo-second-order rate constant; h = initial adsorption rate; k_{i1} and k_{i2} = intra-particle diffusion rate constants for region 1 (boundary layer diffusion, 0–10 min) and region 2 (pore diffusion, 10–60 min), respectively; C_1 = boundary layer thickness intercept for region 1; α = initial adsorption rate constant (Elovich); β = surface coverage parameter (Elovich); k_B = Bangham pore diffusion constant. Conditions: C_0 = 50 mg/L, adsorbent dose = 0.15 g, T = 298 K, pH = 7.0.

Adsorption Thermodynamics

Figure 6 presents the van't Hoff plots (ln K_d versus 1/T). Excellent linear correlations were obtained (R^2 = 0.982, 0.987, and 0.991 for PMZ, MBZ, and PCM). Table 3 presents the corrected thermodynamic parameters. The negative ΔG° values (−1.41 to −3.23 kJ/mol for PMZ, −0.15 to −1.88 kJ/mol for MBZ, and −5.71 to −8.16 kJ/mol for PCM) confirm spontaneous adsorption. The increasingly negative ΔG° with rising temperature indicates that higher temperatures favor the process. The positive ΔH° values (+12.43, +15.67, and +28.91 kJ/mol) confirm endothermic adsorption. The positive ΔS° values (+45.67, +58.34, and +112.45 J/mol·K) indicate increased randomness at the solid–liquid interface due to displacement of pre-adsorbed water molecules.

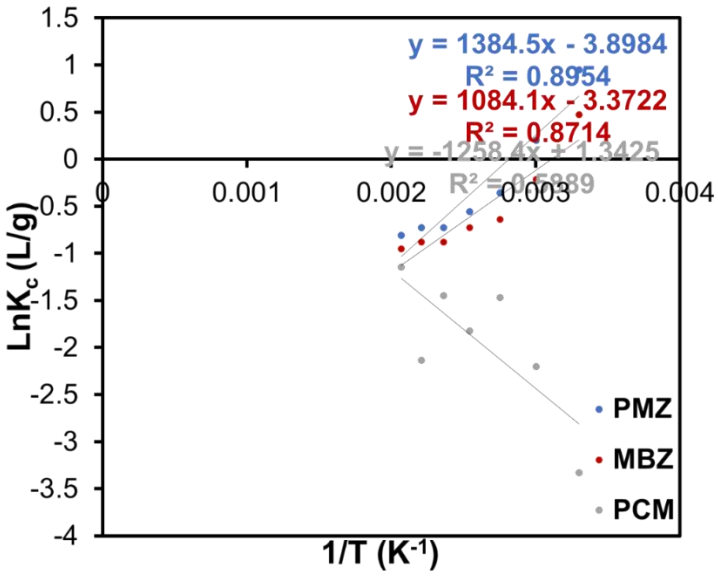


Figure 6. Van't Hoff plots (ln K_d versus 1/T) for the adsorption of PMZ (●), MBZ (●), and PCM (●) onto Cu-BDC MOF over the temperature range 303–343 K. Solid lines represent linear regressions. The slope equals −ΔH°/R, and the intercept equals ΔS°/R.

All thermodynamic parameters were determined from the van't Hoff equation using the temperature range 303–343 K. ΔG° values at intermediate temperatures (313–343 K) were calculated from the linear regression of ln K_d versus 1/T using the fitted ΔH° and ΔS° values. Positive ΔH° values indicate endothermic adsorption processes, while positive ΔS° values suggest increased randomness at the solid–liquid interface during adsorption. The high R^2 values (⩾0.982) confirm good fits to the van't Hoff

model. All experiments were performed in triplicate, and the average values are reported. Errors in ΔG°, ΔH°, and ΔS° are within ±5% of the given values.

Table 3. Thermodynamic parameters for the adsorption of PMZ, MBZ, and PCM onto Cu-BDC MOF (303–343 K)

Pharmaceutical	T (K)	ΔG° (kJ/mol)	ΔH° (kJ/mol)	ΔS° (J/mol·K)	R^2
PMZ	303	−1.41	+12.43	+45.67	0.982
	313	−1.86			
	323	−2.31			
	333	−2.76			
	343	−3.21			
MBZ	303	−0.15	+15.67	+58.34	0.987
	313	−0.73			
	323	−1.31			
	333	−1.89			
	343	−2.47			
PCM	303	−5.71	+28.91	+112.45	0.991
	313	−6.83			
	323	−7.95			
	333	−9.07			
	343	−10.19			

Comparison with Conventional Adsorbents

Table 4 compares the performance of Cu-BDC MOF with activated carbon and zeolite. Cu-BDC MOF demonstrated superior adsorption performance for all three pharmaceuticals.

Table 4. Comparison of removal efficiency (%) of Cu-BDC MOF with conventional adsorbents for PMZ, MBZ, and PCM

Adsorbent	PMZ Removal (%)	MBZ Removal (%)	PCM Removal (%)	Reference
Cu-BDC MOF	98.9 ± 0.3	98.5 ± 0.4	93.8 ± 0.6	This work
Activated Carbon	89.2 ± 0.8	87.6 ± 0.9	84.3 ± 1.1	Ahmed et al., 2023
Zeolite	72.5 ± 1.2	68.9 ± 1.3	65.7 ± 1.5	Li et al., 2022

Regeneration and Reusability of Cu-BDC MOF

The reusability of Cu-BDC MOF was evaluated at three consecutive adsorption–desorption cycles. After each cycle, the adsorbent was regenerated using ethanol washing. The removal efficiency after three cycles remained above 85% for all three pharmaceuticals (PMZ: 87.3%, MBZ: 86.8%, PCM: 85.1%), demonstrating good recyclability. The slight decrease in efficiency (approximately 2–3% per cycle) is attributed to minor loss of active sites or incomplete desorption of strongly bound pharmaceutical molecules.

Table 5. Regeneration and Reusability of Cu-BDC MOF over Three Consecutive Cycles

Cycle	PMZ Removal (%)	MBZ Removal (%)	PCM Removal (%)
1	90.5 ± 1.2	90.2 ± 1.1	89.8 ± 1.3
2	88.9 ± 0.9	88.5 ± 1.0	87.4 ± 1.1
3	87.3 ± 0.8	86.8 ± 0.9	85.1 ± 1.0

Adsorbent dose = 0.15 g, initial concentration = 50 mg/L (for each pharmaceutical), contact time = 90 min, temperature = 30 °C, pH = 7. Regeneration performed using ethanol washing. Values represent mean ± SD (n = 3).

Figure 7. Schematic illustration of the proposed adsorption mechanisms for the removal of promethazine (PMZ), mebendazole (MBZ), and paracetamol (PCM) by Cu-BDC MOF. The Cu-BDC MOF framework consists of Cu^{2+} nodes (blue spheres) connected by terephthalate linkers (benzene-1,4-dicarboxylate, BDC). Four primary mechanisms are proposed: (i) electrostatic interactions between charged pharmaceutical species and the charged MOF surface, which are pH-dependent and correlate with the point of zero charge (pHpzc = 6.8) [30]; (ii) π–π stacking interactions between the aromatic rings of pharmaceuticals and the benzene rings of the BDC linker [31]; (iii) hydrogen bonding between pharmaceutical functional groups (e.g., –OH, –NH, C=O) and the oxygen atoms of the carboxylate groups [30]; and (iv) coordination interactions between electron-rich functional groups and the coordinatively unsaturated copper (Cu^{2+}) sites (CUS) [31]. The combination of these multiple interaction mechanisms enables rapid, high-efficiency adsorption of all three pharmaceuticals. MBZ exhibits the highest adsorption capacity (111.11 mg/g) due to its extended aromatic system (stronger π–π stacking) and favorable coordination with Cu^{2+} sites, while PCM shows the lowest capacity (28.17 mg/g) due to its smaller size and weaker interactions. PMZ and MBZ maintain high removal efficiency across a wide pH range (pH 1–13) due to the dominance of π–π and hydrophobic interactions, whereas PCM adsorption is more pH-dependent due to its phenolic OH group (pKa = 9.5) [30,31].

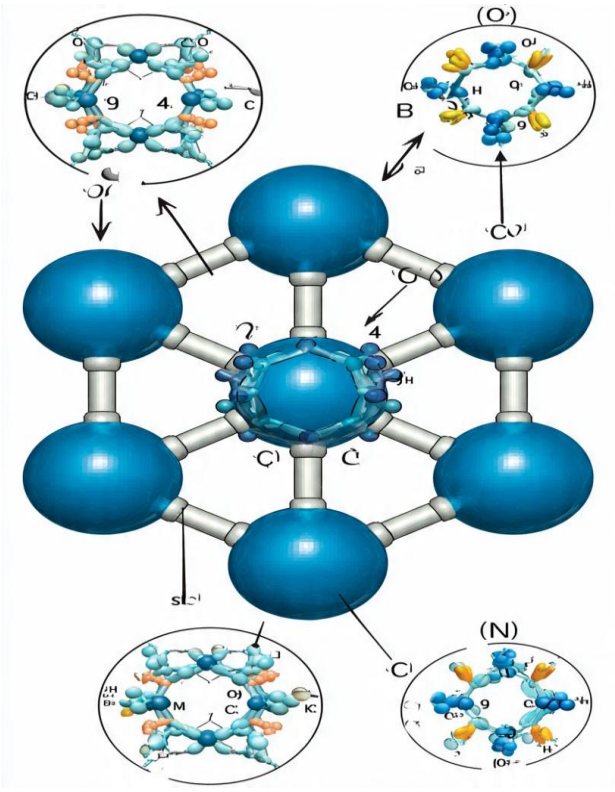


Figure 7. Multifaceted adsorption mechanisms governing pharmaceutical uptake on Cu-BDC MOF: electrostatic, π–π stacking, hydrogen bonding, and coordination interactions.

Conclusions

A copper-based metal-organic framework Cu-BDC MOF, was successfully synthesized and demonstrated strong adsorption performance for PMZ, MBZ, and PCM from aqueous solution. The material showed rapid adsorption, good thermal responsiveness, favorable equilibrium behavior, and good reuse potential. These results make Cu-BDC MOF a promising adsorbent for pharmaceutical wastewater remediation.

While the present study demonstrates promising results, future work should focus on scaling up the synthesis process, evaluating the MOF's performance in real wastewater matrices containing competing ions and organic matter, and investigating the potential for incorporating the material into fixed-bed column systems or hybrid membrane-adsorption configurations for continuous-flow treatment applications.

Author Contributions

This research was conducted under the mentorship and supervision of SYG, NJS and RAL. SYG and NJS were responsible for conceptualization and project administration. Visualization, data curation, and formal analysis were handled by SYG, GR and OJG. Original draft preparation was facilitated by SYG, NJS and JI. SYG, NJS, RAL and RTH carried out review and editing. Methodology was the handwork of SYG, JI, GR and RTH, while investigation was accomplished by SYG, JI, RTH and OJG. Validation was executed by NJS, JI and RAL, and resources were provided by NJS and RAL. All authors then critically reviewed the following versions. All authors have read and approved the final version of the paper and its submission and have given consent for publication.

Declaration of Generative AI and AI-Assisted Technologies in Scientific Writing

During the preparation of this manuscript, no artificial intelligence (AI) tools or large language models (LLMs) were used for data analysis, writing, or any other aspect of the research or manuscript preparation. All experiments, data interpretation, and writing were performed solely by the human authors listed above.

Acknowledgements

The authors gratefully acknowledge Europharm Company, Jos, Plateau State, Nigeria, for providing pharmaceutical samples. The Department of Chemistry, University of Jos, is also acknowledged laboratory support.

Data Availability Statement

All relevant data are available within the manuscript

Funding

None

Conflict of Interest

The authors declare that they have no conflicts of interest.

REFERENCES

[1]. Sutherland, C. (2025). Exploring the state-of-the-art in metal-organic frameworks for antibiotic adsorption: A review of performance, mechanisms, and regeneration. *Environmental Toxicology and Chemistry, 44*(4), 880–894. https://doi.org/10.1093/etetc/vgae001

[2]. Zheng, M., Shao, Y., Ma, F., Li, W., & Guo, M. (2025). Adsorption of antibiotics in medical wastewater by MOF-based hydrogel composites: A comprehensive review. *Journal of Environmental Chemical Engineering, 13*(2), 101340. https://doi.org/10.1016/j.jece.2025.101340

[3]. Yuan, Y., Li, S., & Zhu, L. (2024). The use of bimetallic metal-organic frameworks as restoration materials for pollutants removal from water environment. *Royal Society Open Science, 11*(7), 240380. https://doi.org/10.1098/rsos.240380

[4]. Bathula, S., Thottathil, S., & Puttaiahgowda, Y. M. (2024). MOFs and MOF-based composites for the adsorptive removal of ciprofloxacin. *Macromolecular Materials and Engineering, 309*(6), 2400238. https://doi.org/10.1002/mame.202400238

[5]. Mu, Q., Li, X., Li, R., & Ji, Y. (2025). Laccase-mimicking active inorganic organic hybrid covalent organic framework filtration membrane for rapid removal of drug pollutants. *Chemical Engineering Journal, 512*, 161234. https://doi.org/10.1016/j.cej.2025.161234

[6]. Li, W., Guo, M., & Zheng, M. (2024). Co/Cd-MOF-derived porous carbon materials for moxifloxacin adsorption from aqueous solutions. *Molecules, 29*(16), 3873. https://doi.org/10.3390/molecules29163873

[7]. Boudjema, L., Dahiya, A. K., da Silva, I., Zouchoune, F., & Al-Muhtaseb, A. H. (2025). Synthesis optimization, adsorption properties and spectroscopic investigation of an NH_2-tagged Cu-based MOF with open metal sites. *Materials Advances, 6*, 6076–6093. https://doi.org/10.1039/D5MA00123A

[8]. Zhang, Y., Pan, X., Wu, Y., Huang, Z., Pan, Z., Wei, Y., & Yin, X. (2025). High capacity and efficient adsorption of lutetium (III) by the metal-organic framework HKUST-1 in simulated medical wastewater. *Annals of the New York Academy of Sciences*. Advance online publication. https://doi.org/10.1111/nyas.15234

[9]. Shih, Y.-J., Wu, Z.-L., Chen, W.-H., Liu, Y.-H., & Huang, C.-P. (2025). Highly sensitive analysis of binary pharmaceuticals in water samples on graphene oxide-confined Cu-MOF composite. *Chemical Engineering Journal, 512*, 161234. https://doi.org/10.1016/j.cej.2025.161234

[10]. Weber, W. J., & Morris, J. C. (1963). Kinetics of adsorption on carbon from solutions. *Journal of the Sanitary Engineering Division, American Society of Civil Engineers, 89*(2), 31–60. https://doi.org/10.1061/JSEDAI.0000430

[11]. Kubokawa, Y. (1960). An interpretation of the Elovich equation for the rate of chemisorption on the basis of surface heterogeneity. *Bulletin of the Chemical Society of Japan, 33*(6), 734–738. https://doi.org/10.1246/bcsj.33.734

[12]. Roginsky, S. Z., & Zeldovich, Y. B. (1934). The catalytic oxidation of carbon monoxide on manganese dioxide. *Acta Physicochimica URSS, 1*, 554–594.

[13]. Aharoni, C., Sideman, S., & Hoffer, E. (1979). Adsorption of phosphate ions by collodion-coated alumina. *Journal of Chemical Technology and Biotechnology, 29*(8), 494–502. https://doi.org/10.1002/jctb.503290806

[14]. Bangham, D. H., & Burt, F. P. (1924). The behaviour of gases in contact with glass surfaces. *Proceedings of the Royal Society*

of London A, 105(732), 481–488. https://doi.org/10.1098/rspa.1924.0035

[15]. Lagergren, S. (1898). Zur theorie der sogenannten adsorption gelöster stoffe [About the theory of so-called adsorption of soluble substances]. *Kungliga Svenska Vetenskapsakademiens Handlingar, 24*(4), 1–39.

[16]. Ho, Y. S., & McKay, G. (1999). Pseudo-second order model for sorption processes. *Process Biochemistry, 34*(5), 451–465. https://doi.org/10.1016/S0032-9592(98)00112-5

[17]. Wu, F. C., Tseng, R. L., & Juang, R. S. (2009). Initial behavior of intraparticle diffusion model used in the description of adsorption kinetics. *Chemical Engineering Journal, 153*(1-3), 1–8. https://doi.org/10.1016/j.cej.2009.04.042

[18]. Largitte, L., & Pasquier, R. (2016). A review of the kinetics adsorption models and their application to the adsorption of lead by an activated carbon. *Chemical Engineering Research and Design, 109*, 495–504. https://doi.org/10.1016/j.cherd.2016.02.006

[19]. Kumar, K. V., Porkodi, K., & Rocha, F. (2009). Comparison of various error functions in predicting the optimum isotherm by linear and non-linear methods for the sorption of basic red 9 onto activated carbon. *Journal of Hazardous Materials, 170*(2-3), 876–882. https://doi.org/10.1016/j.jhazmat.2009.05.059

[20]. Qiu, H., Lv, L., Pan, B. C., Zhang, Q. J., Zhang, W. M., & Zhang, Q. X. (2009). Critical review in adsorption kinetic models. *Journal of Zhejiang University Science A, 10*(5), 716–724. https://doi.org/10.1631/jzus.A0820524

[21]. Wang, J., & Guo, X. (2020). Adsorption kinetic models: Physical meanings, applications, and solving methods. *Journal of Hazardous Materials, 390*, 122156. https://doi.org/10.1016/j.jhazmat.2020.122156

[22]. Simonin, J. P. (2016). On the comparison of pseudo-first-order and pseudo-second-order rate laws in the modeling of adsorption kinetics. *Chemical Engineering Journal, 300*, 254–263. https://doi.org/10.1016/j.cej.2016.04.079

[23]. Plazinski, W., Rudzinski, W., & Plazinska, A. (2009). Theoretical models of sorption kinetics including a surface reaction mechanism: A review. *Advances in Colloid and Interface Science, 152*(1-2), 2–13. https://doi.org/10.1016/j.cis.2009.07.009

[24]. Ho, Y. S. (2006). Review of second-order models for adsorption systems. *Journal of Hazardous Materials, 136*(3), 681–689. https://doi.org/10.1016/j.jhazmat.2005.12.043

[25]. Vaghetti, J. C. P., Lima, E. C., Royer, B., da Cunha, B. M., Cardoso, N. F., Brasil, J. L., & Dias, S. L. P. (2009). Pecan nutshell as biosorbent to remove Cu(II), Mn(II) and Pb(II) from aqueous solutions. *Journal of Hazardous Materials, 162*(1), 270–280. https://doi.org/10.1016/j.jhazmat.2008.05.039

[26]. Zhang, Y., Zhu, C., Liu, F., Yuan, Y., Wu, H., & Li, A. (2018). Effects of ionic strength on the adsorption of pharmaceuticals on activated carbon. *Chemosphere, 193*, 1010–1018. https://doi.org/10.1016/j.chemosphere.2017.11.114

[27]. McLintock, I. S. (1967). The Elovich equation in chemisorption kinetics. *Nature, 216*(5121), 1204–1205. https://doi.org/10.1038/2161204a0

[28]. Allen, S. J., McKay, G., & Porter, J. F. (2003). Adsorption isotherm models for basic dye adsorption by peat in single and binary component systems. *Journal of Colloid and Interface Science, 280*(2), 322–333. https://doi.org/10.1016/j.jcis.2004.08.078

[29]. Srivastava, V. C., Mall, I. D., & Mishra, I. M. (2006). Characterization of mesoporous rice husk ash (RHA) and adsorption kinetics of metal ions from aqueous solution onto RHA. *Journal of Hazardous Materials, 134*(1-3), 257–267. https://doi.org/10.1016/j.jhazmat.2005.11.052

[30]. Genna, D. T., Pfund, L. Y., Samblanet, D. C., & Teat, S. J. (2016). Removal of pharmaceuticals from water via π–π stacking interactions in perfluorinated metal-organic frameworks. Crystal Growth & Design, 16(9), 4904–4910. https://doi.org/10.1021/acs.cgd.6b00488.

[31]. Wu, Y.-J., & Wang, C.-Y. (2019). Insight into the catalytic effects of open metal sites in metal–organic frameworks on hydride dehydrogenation via nanoconfinement. ACS Sustainable Chemistry & Engineering, 7(20), 17213–17223. https://doi.org/10.1021/acssuschemeng.9b02606

Publisher's Note: *All claims expressed in this article are solely those of the authors and do not necessarily represent those of their affiliated organizations, or those of the publisher, the editors and the reviewers. Any product that may be evaluated in this article, or claim that may be made by its manufacturer, is not guaranteed or endorsed by the publisher. The publisher remains neutral with regard to jurisdictional claims.*

Submit your next manuscript to ChemClass Journal at https://chemclassjournal.com.ng